Processing and Application of Ceramics 12 [2] (2018) 153–163
https://doi.org/10.2298/PAC1802153G

Electrical properties of calcium doped $BiFeO_3$ films on $LaNiO_3$ coated Pt substrates

Lucas Fabricio Goncalves[1], Leandro Silva Rosa Rocha[1], Bruno Hangai[1], Pedro Paulo Silva Ortega[1], Elson Longo[2], Alexandre Z. Simões[1,*]

[1]*Sao Paulo State University (Unesp), School of Engineering, Guaratinguetá, Brazil*
[2]*Sao Paulo State University (Unesp), Institute of Chemistry, Araraquara, Brazil*

Received 31 January 2018; Received in revised form 13 May 2018; Accepted 27 May 2018

Abstract

Pure and calcium-modified ($Ca_xBi_{1-x}FeO_3$, x = 0.0, 0.1, 0.2, 0.30) thin films were fabricated on Pt(111)/Ti/SiO_2/Si substrates by the soft chemical method using $LaNiO_3$ as the bottom electrode. Highly (200)-oriented BFO film was coherently grown on LNO at 500 °C. Ca-doped $BiFeO_3$ films have a dense microstructure and rounded grains. The conventional problem of the leakage current for the highest doped film was reduced from 10^{-5} to 10^{-10} with remarkable improvement in the film/electrode interface, chemical homogeneity, crystallinity, and morphology of the BFO film. Enhanced ferroelectricity was observed at room temperature due to the bottom electrode. Fatigue-free films were grown on $LaNiO_3$ bottom electrodes with no degradation after 1×10^{10} switching cycles at an applied voltage of 5 V with a frequency of 1 MHz. After several tests the capacitors retained 77% of its polarization upon a retention time of 10^4 s. Room temperature magnetic coercive field measurements indicate that the magnetic behaviour is influenced by the nature of the bottom electrode.

Keywords: *bismuth ferrite, multiferroics, lanthanum nickelate, thin films*

I. Introduction

Perovskite oxides (ABO_3) have been widely studied as bottom electrodes for the growth of films with ferroelectric and piezoelectric properties [1–4]. These electrodes are replacing platinum electrodes that have been extensively used. However, perovskites have disadvantages such as poor adherence on the Si substrate. This leads to ferroelectric fatigue due to the deficiency in oxygen concentration. Another problem is the difficulty to obtain texturing of thin films on metal structures [1]. The $LaNiO_{3-\delta}$ (LNO) is among the most studied material as an oxide electrode, with a wide range of applications due to two parameters: i) the pseudo-cubic or rhombohedral crystal structure with lattice parameter values close to many ferroelectric materials, and ii) an intrinsic metallic behaviour. The intrinsic metallic behaviour is described by two aspects. The first refers to the strong covalent interaction between the 3*d*-2*p* orbitals of the Ni–O, where Ni^{3+} cations have a low configuration spin of the $3d^7$ ($t_{2g}^6 e_g^1$). Thus, there is the formation of a conduction band (σ^*) between the orbitals e_g of the low hybridization spin of the nickel and *p*-orbitals from oxygen [5], demonstrating that this material presents electronic conductivity. The second aspect refers to the crystalline structure of the $LNiO_3$-family (where L is a lanthanide), where all of them present orthorhombic structure. The $LaNiO_3$ is the single member with rhombohedral structure and high tolerance factor that measures the stress and compression about the binding - AO and BO in the perovskite structure [6].

In previous work, we have shown that the measured leakage current density at 5.0 V for the $Ca_{0.3}Bi_{0.7}FeO_3$ (BCF030) film decreases to 10^{-9} A/cm^2 indicating that the main carrier type which produces observed transport behaviour must be electronic rather than ionic in nature. This suggested that the conduction in calcium substituted $BiFeO_3$ is mainly governed by thermally activated hopping of electrons between oxygen vacancies which is inconsistent with the vacancy assisted electronic conduction mechanism observed in epitaxial thin films [7]. The formation of impurity phases, such as $Bi_{25}FeO_{39}$ and $Bi_2Fe_4O_9$, provides an additional difficulty in the physical characterization of the paraelec-

*Corresponding author: tel: +55 12 3123 2228,
e-mail: *alezipo@yahoo.com*

tric high-temperature phase [8]. Since part of the problem lies in the volatility of bismuth, doping the A site (Bi site) in $BiFeO_3$ is a key strategy, and there have been some studies on the effect of the replacement of Bi3+ with different atoms [9–12]. The doping experiments with Ca^{2+} are of particular interest because they can be exploited to control the band-filling in insulating $BiFeO_3$ thin films, thereby triggering an insulator-metal transition with varying composition [13]. Fatigue-free Ca-doped BFO films have been grown on $Pt/Ti/SiO_2/Si$ substrates. However, a possible interfacial reaction between platinum and bismuth can lead to undesired electrical properties [14]. Therefore, the substitution of metallic electrodes based on noble metals like platinum by conductive oxides is an alternative to reach better electrical properties caused by the high oxygen affinity of these electrodes [15]. It is well known that perovskite oxide electrode, such as $SrRuO_3$, $LaNiO_3$, and $BaPbO_3$, effectively improve crystal growth and electric properties of ferroelectric oxide [16–20]. The specific characteristics of the $LaNiO_3$ electrode are low preparation temperature, good conductivity and chemical stability. Most interestingly, the $LaNiO_3$ electrode could induce the preferred orientation and improve the film/electrode interface. The performance of ferroelectric films is often dominated by the film/electrode interface. In particular, Y. Hou *et al.* [21] demonstrated a large piezoelectric response induced by the coexistence of low-symmetry and self-polarization in Li^+-Nb^{5+}-doped BFO polycrystalline films obtained by the RF-sputtering onto $LaNiO_3$-buffered $Pt/Ti/SiO_2/Si$ substrate, with d_{33} coefficient of 114.1 pm/V, comparable to lead-based piezoelectric films. Bilayered thin films $(Ba(Zr_{0.2}Ti_{0.8})O_3-0.5\,(Ba_{0.7}Ca_{0.3})TiO_3$, i.e. BZT-0.5BCT) were also prepared by the dual-magnetron sputtering on $LaNiO_3$ seed layer, showing d_{33} coefficient of 122 pm/V along with a dielectric constant (ε_r) of 1046 [22].

To the best of our knowledge, no report is available on the film/electrode interface of BFO films obtained by the polymeric precursor method (PPM). Therefore, we expect that $LaNiO_3$ as the metal oxide bottom electrode could provide a template to grow high quality films with preferred orientation.

II. Experimental procedure

Ca-modified $BiFeO_3$ and the $LaNiO_3$ thin films were prepared by the PPM as described elsewhere [23]. Films were spin coated on LNO coated $Pt/Ti/SiO_2/Si$ substrates by a commercial spinner operating at 5000 rpm for 30 s (spin coater KW-4B, Chemat Technology). Each layer was pre-fired at 300 °C for 1 h in a conventional oven. After the pre-firing, each layer was crystallized at 500 °C for 2 hours. Using the same procedure, the multiferroic films were deposited by spinning the precursor solution on the desired substrates. Through this process, we have obtained thickness values of about 150 nm (5 layers) for the bottom LNO electrodes which were crystallized at 700 °C for 2 h, and around 300 nm for BFO (10 layers), reached by repeating the spin-coating and heating treatment cycles. An excess of 5 wt.% of Bi was added to the solution to minimize bismuth loss during thermal treatment. Different $Ca_xBi_{1-x}FeO_3$ samples were prepared and denoted as BFOCax, where x indicates the level of Ca-doping (i.e. x = 0.0, 0.1, 0.2 and 0.30).

Phase analysis of the films was performed at room temperature from X-ray diffraction (XRD) patterns recorded on a Rigaku-DMax 2000PC with Cu-Kα radiation in the 2θ range from 20° to 60° with 0.3°/min steps. The annealed thin film thicknesses were determined using scanning electron microscopy (SEM, Topcom SM-300) by checking their cross-section where backscattered electrons were utilized. Three measurements were taken to obtain an average thickness value. The morphology of the films was observed using a high resolution FEG-SEM (Supra 35-VP, Carl Zeiss, Germany). After deposition of the top electrode, the film was subjected to a post-annealing treatment in a tube furnace under an oxygen atmosphere at 300 °C for 1 h. Here, the desired effect was to eventually decrease oxygen vacancies' content. The *J-E* measurements were recorded on the Radiant Technology tester in the current-voltage mode, with a voltage change from 0 to +10 V, from +10 to −10 V and back to 0 V. The hysteresis loop measurements were carried out on the films with a Radiant Technology RT6000HVS at a measured frequency of 60 Hz. These loops were traced using the Charge 5.0 program included in the software of the RT6000HVS in a virtual ground mode test device. Magnetization measurements were done by using a vibrating-sample magnetometer (VSM) from Quantum Design™. For the fatigue measurements, internally generated 8.6 μs wide square pulses were used. After the end of each fatigue period, the polarization characteristics of the films were measured over a range of frequencies. Retention characteristics of the films were measured by independently observing the time-dependent changes of P^* (switched polarization), and $P^\wedge$ (non-switched polarization). For P^*, the capacitor was switched with a negative write pulse and read by a positive read pulse after retention time t. For $P^\wedge$, positive pulses were used for both writing and reading. The pulse width for all triangular pulses was 1.0 ms. The time delay between the written pulse and the first read pulse is referred to as retention time.

III. Results and discussion

Figure 1 illustrates XRD patterns of the BFO and Ca-doped BFO films deposited on LNO substrates. For comparison, the highest doped film deposited on platinum coated silicon substrate was also presented. The films were well crystallized at 500 °C. The BFO and Ca-doped BFO films were self-organized to produce (200)-preferred orientation with good crystallinity. The

BCF030 film has a tetragonal structure with a *P*4*mm* space group while the BFO film has a rhombohedral structure with an *R*3*c* space group, which can be treated as a special triclinic structure [24]. The XRD pattern of the pure $BiFeO_3$ on Pt shows a rhombohedral lattice similar to the patterns previously reported for pure $BiFeO_3$ [25,26]. The XRD pattern of the BFOCa030 on Pt is similar to those expected for Ca^{2+} doped bismuth ferrite, showing a coexistence of the rhombohedral along with the tetragonal (*P*4*mm*) structure, treated as pseudo-cubic with a four-fold symmetry and a large distortion within the crystal domain [27,28]. The LNO layer not only serves as a useful metal oxide bottom electrode, but also forms a template with preferred (200) orientation to enable growth of high quality BFO films (Fig. 1b-e). As seen in XRD patterns of Ca-doped BFO films, the 110 peak tend to decrease its intensity while the 200 peak is enhanced, likely meaning that the Ca-doped BFO films consisted of single-phase polycrystalline materials with preferred orientation. This is an interesting result considering that the lattice mismatch between LNO (a = 0.384 nm) and BCF030 (a = 0.5578439 nm, c = 1.328924 nm) is considerable. The positive role of LNO may be caused by the decrease in the nucleation activation energy that allows obtaining a good crystallization at this temperature. Ca^{2+} replaces Bi^{3+} only in a perovskite-type unit cell which causes a distorted structure. The distortion increases with a higher Ca content, as shown at 2θ around 36°, presenting an increase mostly related to the 006 peak accompanied by Ca^{2+} addition [14,29,30]. The covalent interaction, which originates from the strong hybridization between Fe 3*d* and O 2*p* orbitals, plays an important role in the structural distortion of the BFO lattice. It can be inferred that Ca improves oxygen ion stability in the lattice because some of the Bi ions in the pseudo-perovskite layers containing Fe–O octahedra are substituted by the divalent ion reducing the *c*-axis. Also,

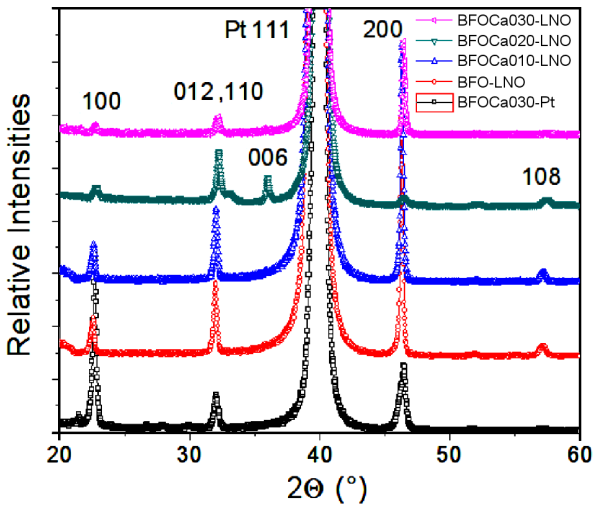

Figure 1. X-ray diffraction of thin films (BFOCa030-Pt, BFO-LNO, BFOCa010-LNO, BFOCa020-LNO and BFOCa030-LNO) annealed at 500 °C in static air for 2 h

the addition of Ca has a radial substitution effect higher than bismuth and stabilizes oxygen vacancies and consequently the structure due to the differences in charge densities of Ca and Bi atoms.

The morphology of the BFO and Ca-doped BFO thin films was evaluated by FEG-SEM measurements (Fig. 2). Changes in the surface of the Ca-doped BFO films were evaluated and the results reveal that the BCF030 film consists of a homogeneous surface, although the BFO film has a high degree of agglomerates. It was also found that the Ca dopant tends to suppress grain growth. The average grain size is 63 nm for the BFO film and 33 nm for the BCF030 film. The surface morphology of the synthesized BFO-based films was improved with high Ca-doping because this improves nucleation and growth process and produces film with a homogeneous and dense microstructure. On the other hand, for low and middle Ca concentrations, the surface consists of irregularities, which were caused by distortion in the lattice caused by Ca addition. The substitution of Ca^{2+} for Bi^{3+} in $BiFeO_3$ can produce oxygen vacancies, which apparently induce distortions and cause structural irregularities within the crystallites. Also, the homogeneous microstructure of the BCF030 films may affect ferroelectric properties because the voltage can be uniformly applied on them. Because of the employed annealing conditions, the diffusion of species and the nucleation and growth rate increased affecting the grain size and shape of grains. Bismuth-based materials contain bismuth metal in the as-deposited films, which also may play an important role in the formation of smooth and dense morphologies.

A strongly marked difference in the film morphology can be observed for the different bottom electrodes. The BCF030 films obtained on Pt coated substrates present a porous perovskite structure while the ones obtained on oxide electrode showed dense films with spherical grains. For films deposited on LNO, the amount of charge carriers (oxygen vacancies), trapped near the film-electrode interface, are minimized. These charges may be originated during the heat treatment process due to the decomposition of the polymeric precursor. It can be assumed that if oxygen vacancy accumulation near the film-electrode interface occurs during the heat treatment, the conductive oxide can consume the oxygen vacancies by changing their oxygen nonstoichiometry and thus, the accumulation of oxygen vacancies near the interface is prevented or reduced affecting the shape and size of grains. The main reason influencing the surfaces of the BFO films deposited on Pt and the LNO coated Pt substrates can be originated from the difference in nuclei generation density between the Pt and LNO electrodes. After formation of the BFO film, the buffer layer disappears indicating that this conductive oxide acts not as a barrier layer, but as an initial nucleation aid for the multiferroic thin film with a very noticeable phase transition. Thus, the lower grain size obtained in doped samples reflects an increase in the crystallization tempera-

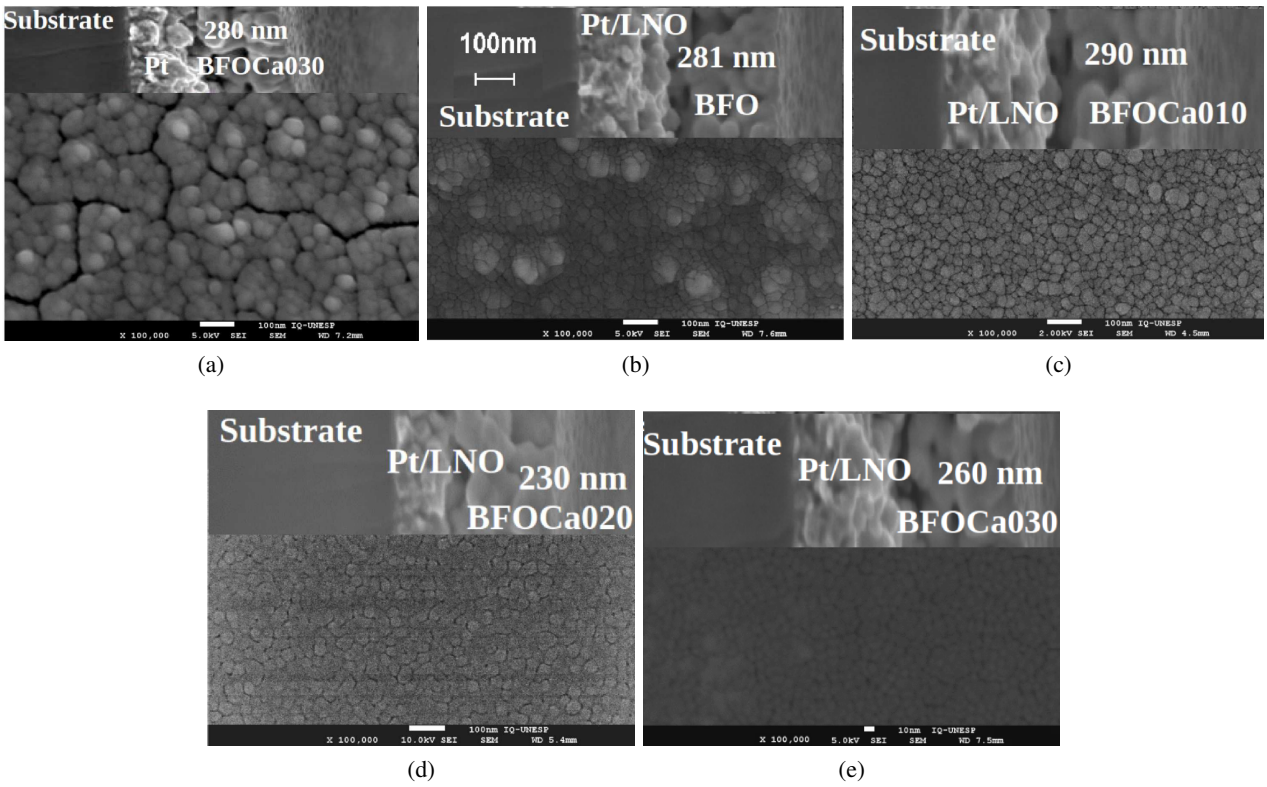

Figure 2. FEG-SEM micrographs of thin films deposited by the polymeric precursor method and annealed at 500 °C in static air for 2 h: a) BFOCa030-Pt, b) BFO-LNO, c) BFOCa010-LNO, d) BFOCa020-LNO and e) BFOCa030-LNO

ture due to the differences in chemical bond strengths between Fe–O and Ca–O atoms.

Figures 3a-e show the leakage current density as a function of voltage measured at room temperature. The curve was recorded with a voltage step width of 0.1 V and elapsed time of 1.0 s for each voltage. The measured current densities (J) versus the applied electric field (E) show two clearly different regions. The insulating properties of the films were found to be dependent on the bottom electrode. The leakage current density decreased for the films deposited on the LNO bottom electrode. Such a reduction in leakage current density may be attributed to the high oxygen affinity of the bottom electrode avoiding oxygen depletion in the electrode material caused by the ferroelectric material, thus leaving an oxygen deficient layer of the electrode at the interface and increasing the contact resistance. Also, it may be attributed to the reduction of the number of electrons injected from the cathode at a rate faster than they can travel through the film. A low threshold electric field was applied in order to overcome the larger repulsion forces that are due to the increased amount of non-neutralized charges in the traps of the multiferroic film. The current density increases linearly with the external voltage in the region of low applied voltage strengths, which suggests an ohmic conduction. At higher field strengths, the current density increases exponentially which implies that at least one part of the conductivity results from the Schottky or Poole-Frenkel emission mechanism, except for the BFOCa030 film which kept it practically constant. The leakage current density at 5.0 V (~1.92×10^9 V/cm for LNO; ~10^9 V/cm for Pt) for the BFOCa30 film changes from 10^{-5} A/cm^2 (Pt) to extremely reduced values, below 10^{-9} A/cm^2 (LNO). The main reason for such a small value can be attributed to changes in the surface roughness and the reduction of micropores due to the modification of the interface stability on oxide electrode. Thus, the bottom electrode reduces oxygen vacancies improving switching process of ferroelectric domains. Other reason for this is that introduction of LNO as a bottom electrode reduces grain sizes of the film as evidenced by FEG-SEM, leading to an increase in the density of grain boundaries, which makes contribution to the decreased leakage current density. Normally, the mobile oxygen vacancies are donor like trapping centres for electrons. The energy levels associated with $V_O^{\bullet\bullet}$ are very close to the conduction band. Therefore, the electrons can be readily activated to be free for conduction by the electric field. However, the electric field required for generation of the free electrons in BFO-based film may be increased if complex cluster defects between the vacancies are formed, since the applied electric field has to overcome the electrostatic attraction force between $V_O^{\bullet\bullet}$ and $V_{Bi}^{'''}$ before the oxygen vacancies become mobile and can serve as the trapping centres for electrons. Note that the different positions occupied by $V_{O^{2-}}^{\bullet\bullet}$ in perovskite octahedral will result in different electrostatic forces between $V_{Bi}^{'''}$ and $V_{O^{2-}}^{\bullet\bullet}$, which in turn lead to the different electric fields required for breaking the defect com-

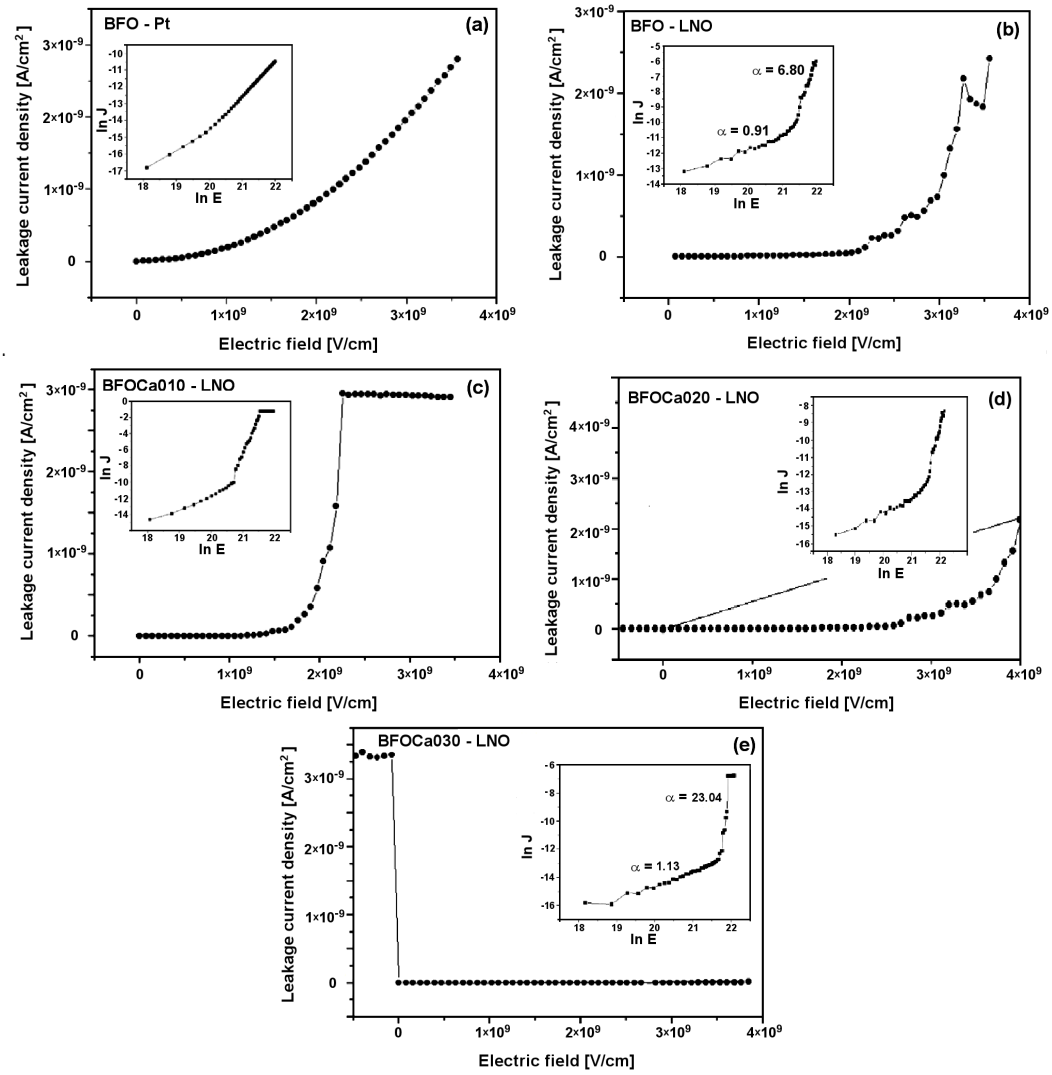

Figure 3. *J-E* curves of thin films annealed at 500 °C in static air for 2 h: a) BFOCa030-Pt, b) BFO-LNO, c) BFOCa010-LNO, d) BFOCa020-LNO and e) BFOCa030-LNO

plexes. Based on the above discussion, the high leakage current in the film deposited on Pt compared to that deposited on LNO may result from the formation of defect complexes between $V_{Bi}^{'''}$ and $V_{O^{2-}}^{\bullet\bullet}$. Thus, the increase of the leakage current with the electric field can be ascribed to the gradual release of $V_{O^{2-}}^{\bullet\bullet}$ from the complexes of $V_{Bi}^{'''}$-$V_{O^{2-}}^{\bullet\bullet}$. As observed, the films deposited on Pt have a rounded shape grains with residual porosity which might have lots of carrier traps. In the low E region, carriers are localized around the traps reducing *J*. In the high *E* region, the localized carriers begin to come out of the trap, resulting in a large increase of *J*. Therefore, a large leakage current was observed in the film with a porous microstructure due the lots of carrier traps inside it and for higher fields these charges are ejected. This behaviour suggests that the Schottky or Poole-Frenkel emission conduction models can dominate in these films. In the porous grain structure of the films, Schottky or Poole-Frenkel emission conduction from traps in high fields looks like the most effective origin of the nonlinear behaviour. On the other hand, in a dense structure, carrier injection into the insulator looks very important, so space charge can be distributed along multiple grain boundaries.

In order to analyse the main dominant mechanism in all films at higher fields, the *J-E* properties should be plotted using Schottky (SE) and Poole-Frenkel (P-F) emission models. The former is emission process across the interface between a semiconductor (metal) and an insulating film as a result of barrier lowering due to the applied field and the image force. The latter is associated with the field enhanced thermal excitation of charge carriers from traps, sometimes called the internal Schottky effect. These two transport mechanisms are very similar and can be distinguished from the slope measured from the straight line region of the current-voltage (*I-V*) curve in the form of a ln *J vs* ln *E* plot. According to literature data [31], the curves of all films can be modelled in terms of space charge-limited current (SCLC).Once in the low field region, the curves follow ohmic conduction properties ($\alpha \sim 1$).With the increase in electric field, a change in α takes place, in

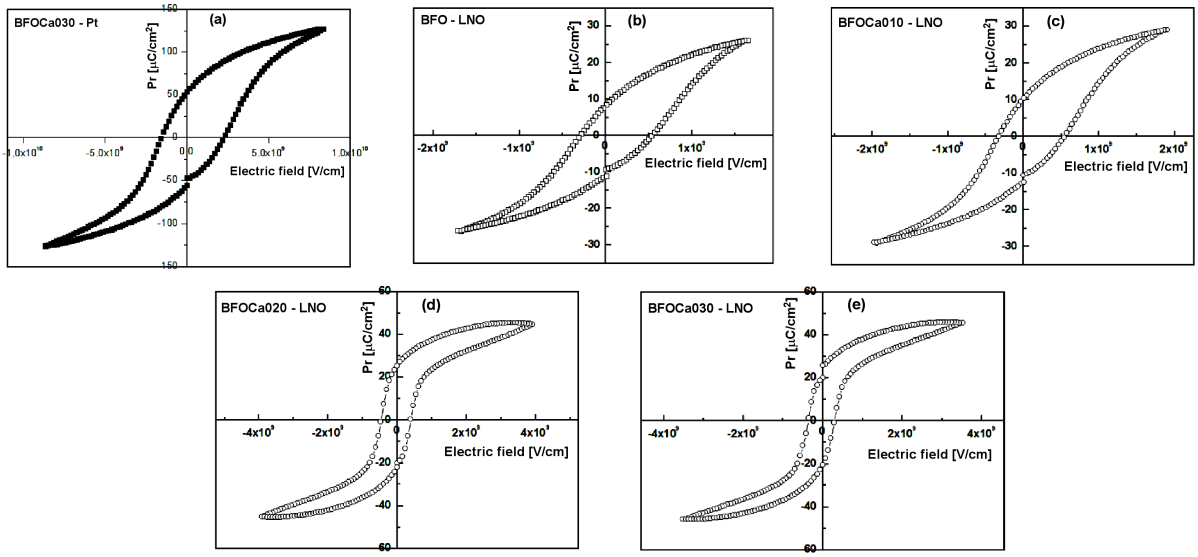

Figure 4. Hysteresis loops of thin films annealed at 500 °C in static air for 2 h: a) BFOCa030-Pt, b) BFO-LNO, c) BFOCa010-LNO, d) BFOCa020-LNO and (e) BFOCa030-LNO

agreement with the modified Child's law conduction. When the electric field is further increased, a sharp increase in the slope occurs because of more complex conduction mechanisms. The change in the transition electric field region corresponding to the conduction mechanism may be due to the electrode interface traps, grain boundary defects and oxygen vacancies.

The room temperature *P-E* hysteresis loops of BFO and Ca-doped BFO thin films are shown in Figs. 4a-e. No sign of leakage has been observed under a measuring frequency of 60 Hz. Low coercive fields could be expected for the film with bottom Pt electrode and this could result in a higher concentration of defects and higher leakage. For that reason, a couple of films were prepared on LNO bottom oxide electrodes to minimize formation of oxygen vacancies. The coercive field along the (200) orientation is smaller than the polarization of the (110) orientation. The *P-E* hysteresis loop of the BCF030 on Pt shows remnant polarization, P_r, of 52 μC/cm^2 after applying 28 V. This high value is not intrinsic, but is induced by high leakage in this structure, as indicated by the roundish shape of the *P-E* loop. Additionally, space charges can also contribute to the polarization. The loops of the films deposited on LNO bottom electrode are well saturated and rectangular with P_r ranging from 8.4 to 22 μC/cm^2 after applying a voltage of less than 10 V.

Since the films on LNO electrode are intensely (200) oriented we reasonably expect a larger polarization. A moderate coercive field probably originates from the intermediary grain size (45 nm) of the layers deposited on LNO electrode. Even the BFOCa30 film deposited on Pt electrode shows a symmetric hysteresis curve probably originating from the local distortion and strain caused by the rhombohedral co-existing phase and reflected in physical properties of the tetragonal phase. Adding Ca^{2+} ions to BFO in high concentrations requires charge compensation, which can be achieved by the formation of Fe^{4+} or oxygen vacancies. If Fe^{4+} exists, the statistical distribution of Fe^{3+} and Fe^{4+} ions in the octahedron may also lead to strong polarization while high coercitivity can be caused by the pinning of ferroelectric domain walls which results from the ferroelectric anisotropy. The low polarization could be addressed to the trapped charge ($O_2^{''}$) associated with other defects ($V_O^{\bullet\bullet}$) or even defect dipole complexes such as oxygen vacancies associated with bismuth vacancies ($V_{Bi}^{'''}$ - $V_O^{\bullet\bullet}$) located at the grain boundary. The film-electrode interface can promote a local stoichiometry deviation influencing the switching of only one component of electrical polarization. As a consequence of these space charges, a significant increase of the electric field is evident, which may lead to a failure of the capacitor. The film deposited on Pt electrode exhibits a poor *P-E* hysteresis loop, which has been typically observed from conductive ferroelectrics and it got broken with increased bias electric field due to a large leakage current. The ferroelectric properties may be related to the decreased grain size with Pt electrode, since the strength of polarization is strongly related to the grain size [32]. It has been found that the polarizability in perovskites (ABO_3) is partially related with the sizes of A and B cations. In general, a large A cation results in an increase in polarizability, since the large A cation leads to "a larger rattling space" available for B cation by increasing the size of the oxygen octahedron. The increased remnant polarization of the films deposited on LNO bottom electrode can be explained by the inhibition of defect complexes between $V_{Bi}^{'''}$ and $V_{O^{2-}}^{\bullet\bullet}$. In the case of the film deposited on Pt electrode, the decreased volume fraction of dielectric polarization with decreasing grain size could have predominant effect on the remnant polarization. A more symmetric hysteresis loop is observed for the film deposited on LNO electrode in-

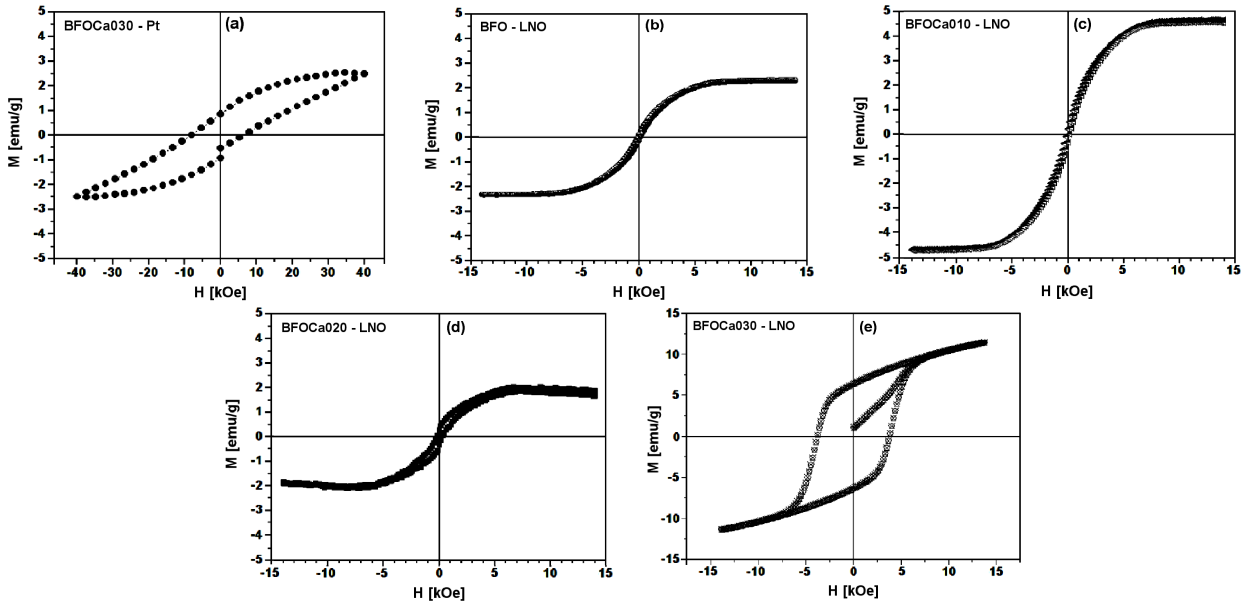

Figure 5. Field dependencies of the magnetization of thin films annealed at 500 °C in static air for 2 h: a) BFOCa030-Pt, b) BFO-LNO, c) BFOCa010-LNO, d) BFOCa020-LNO and (e) BFOCa030-LNO

dicating that the high oxygen affinity of this material avoids the migration of charge species to the electrode-film interface. This behaviour can be ascribed to the larger grains of the films deposited on LNO bottom electrode. The domain walls in larger grains are easier to be switched under external field. Similar phenomena have been found in $SrBi_2Ta_2O_9$ and $PbTiO_3$ thin films [33,34]. The polarization switching in films with small grains is usually more difficult, as in the case of BCF030 on LNO. Therefore, the growth of the film in one direction not coincident with (110) preferred orientation will favour smaller grains morphology, such as the ones grown on LNO bottom electrode leading to a lower E_c when compared to those grown on Pt.

Magnetizations (M) versus field (H) loops were recorded at 300 K (Figs. 5a-e). The BCF030 film deposited on Pt coated substrate exhibits hysteresis loop with a saturation magnetization of 2.5 emu/g and coercive field (H_c) of 1.8 kOe. The ferromagnetic response suggests that the magnetic behaviour is influenced by the crystal size as M_s has been reported to drop with the reduction in the crystal size [20,35]. On the other hand, saturation magnetization of the films deposited on LNO bottom electrode are around 6.0 emu/g with a coercive fields (H_c) of 3.8 kOe. The possible origins of the difference in magnetic properties are mainly attributed to several factors. One is the variation of grain size. As it is well known, the particle size has been reported to influence the magnetic properties of the materials. Here, the crystallite sizes of all films are below 62 nm, where the spiral spin structure is destroyed, which will lead to the uncompensated spins existence at the crystallite surface and in turn it results in the appearance of the uncompensated spins at the grain boundary [36]. Additionally, the effect of texture difference resulting from magnetic annealing should be considered. Other possible reasons for this enhancement in magnetization are: i) the spatial homogenization of the spin arrangement [37]; ii) the distorted spin cycloid structure when LNO is introduced as bottom electrode [38]; iii) the formation of partial Fe^{2+}; iv) the varied canting angle of the Fe–O–Fe bond [39] or v) the increased tensile strain changing the balance between the antiferromagnetic and ferromagnetic interactions [40]. However, the magnetization difference observed in the films may not be attributed to the crystallite size since all the crystallites have almost the same size, as shown in Fig. 2. Nevertheless, with decrease in the grain boundary due to the increase in the applied annealing field, the uncompensated spins at the grain surface reduce. As a result, the magnetization of the fields-annealing thin films is lower than the non-field-annealing one. The other factor is the degree of the crystallite rotation and alignment along the annealing field direction. Applying magnetic field during the annealing process can improve the connection and diffusion of components as well as rotating the crystals to align along the annealing field direction [41]. Such rotation and alignment of the crystallites result in the enhancement of magnetization. Generally, decreasing uncompensated spins at the grain boundary and increasing alignment degree of the BFO crystallites with increasing annealing field lead to the magnetization. Magnetic interaction between different grains decreases initially and then increases, which further results in the same variation of the spinglass transition temperature [42]. Since LNO bottom electrode results in better magnetic response, it is reasonable to believe that if oxygen vacancy accumulation near the film-electrode interface occurs during measurement, the conductive oxide can provide the oxygen to those vacancies by changing their oxygen nonstoichiometry and thus, the accumulation of oxygen vacancies near the interface is prevented

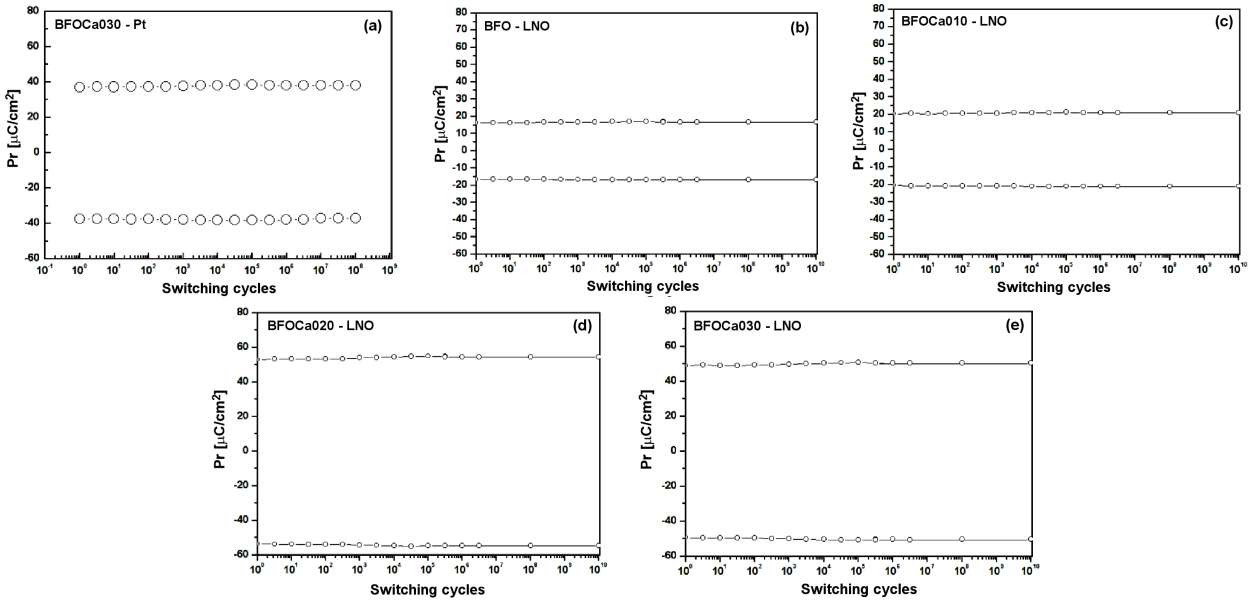

Figure 6. Fatigue behaviour of thin films annealed at 500 °C in static air for 2 h: a) BFOCa030-Pt, b) BFO-LNO, c) BFOCa010-LNO, d) BFOCa020-LNO and (e) BFOCa030-LNO

or reduced. On the other hand, films deposited on Pt electrode reveal an increase in local current around the nucleation sites which can damage the film-electrode interface and suppress the nucleation of oppositely oriented domains at the surface. The film deposited on Pt can provide conductive electrons which reduce the polarization and increase the concentration of holes in the interface region. On the other hand, the LNO bottom electrode can maintain the stability of the interface and bulk defects and solve the weak ferromagnetism. Thus, the film with the highest Ca-doping is ferromagnetic at RT having maximal reminiscent magnetization and coercive field. Although the reason behind the occurrence of FM in the Ca-doped BFO samples is not clearly understood, this can be attributed to the change in interaction between Fe_3^+ and Fe_4^+ breaking down the balance between the antiparallel sublattice magnetization [43]. Change in canting angle [44] or spiral spin modulation [31] may also be responsible for this phenomenon.

The fatigue endurances of the pure and Ca doped BFO thin films were tested at 1 MHz as a function of switching cycles by applying 8.6 μs wide bipolar pulses with maximum amplitude of 9 V (Figs. 6a-e). P^* is the switched polarization between two opposite polarity pulses and $P\wedge$ is the non-switched polarization between the same two polarity pulses. The $P^* - P\wedge$ or $P^* - (-P\wedge)$ denote the switchable polarization, which is an important variable for non-volatile memory application. We claim that calcium stabilizes the charged domain walls which interact with oxygen vacancies and inhibit fatigue. During fatigue, an accumulation of oxygen vacancies near the electrode-film interface can occur, which reduces the effective applied electric field. This fact is well-reflected in fatigue measurements (Figs. 6a-e), that clearly show that even after 10^{10} switching cycles, no decay in the remnant polarization is present for all investigated films. The substitution of Ca for Bi can change the chemical environment of the perovskite layers and solve the fatigue problem of the pure BFO thin films. Since a Ca^{3+} ion has no outer electron, in contrast to a Bi^{3+} ion, which has a lone pair of 6*s* electrons, less hybridization with O 2*p* should lead to less structural distortion favouring the improvement of its ferroelectric properties. The maximum amplitude of 9 V was applied to all films taking into account that the BFOCa30 film presents low coercive field which is employed as a tool for fatigue endurance. The marked improvement in the fatigue behaviour of LNO bottom electrode may result from the crystallinity, electrode/ferroelectric interface and defect concentration. In the interface region the conductive oxide results in less charge trapping and domain wall pinning. Therefore, the effect of the LNO electrode which is a metallic oxide on the fatigue behaviour of the multiferroic films may be attributed to its function as an oxygen vacancy trap.

Retention, which is the time dependent change of the polarization state of the ferroelectric film, is another factor which limits the life of a ferroelectric memory device. Ferroelectric retention properties were measured at room temperature using a Radiant Technology RT6000 A test system (Figs. 7a-e). At first, a triangular pulse of −5 V was applied to write a known logic state, then, after a predetermined time, the logic state was sequentially read by applying two triangular pulses of +5 V and −5 V. The pulse width for all triangular pulses is 1.0 ms. Time delay between the write pulse and the first read pulse is called the retention time. The capacitor poled with a negative voltage pulse corresponds to the binary digit "1". Similarly the state "0" was written by poling the capacitor by applying a positive pulse and read after a predetermined time interval r with a positive pulse. Figure 7a shows the retention characteristics of

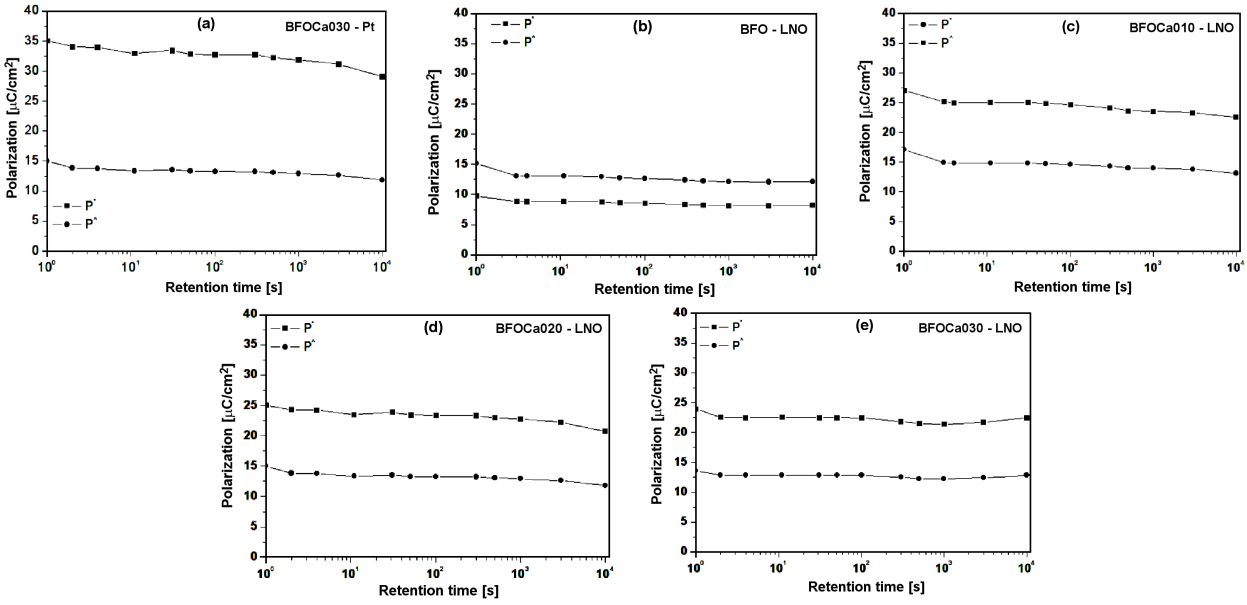

Figure 7. Retention characteristics of thin films annealed at 500 °C in static air for 2 h: a) BFOCa030-Pt, b) BFO-LNO, c) BFOCa010-LNO, d) BFOCa020-LNO and (e) BFOCa030-LNO

the BFOCa030 films, where the retained switchable polarization $P = (P^*)-(P\text{^})$ was plotted as a function of retention time from 1 s to 1×10^4 s at applied electric field of 150 kV/cm. The value of initial polarization decayed and approached a nearly steady-state value after a retention time of 10 s. The corresponding hysteresis loops obtained after the retention test were also essentially identical to that observed before the retention test, indicating that the switchable polarization has almost no loss and the structures have little or no tendency to imprint after 1×10^4 s. The small decay of the retained charge in Ca-doped BFO thin films deposited on LNO bottom electrode even after about 1×10^4 s is a favourable indication for memory applications. The long-time retention characteristics of the Ca-doped BFO thin films are shown in Figs. 7b-e. The overall retention time dependence of polarization retention is quite good. After a retention time of 1×10^4 s, the polarization loss was only about 6% of the value measured at $t = 1$ s for an applied electric field of 150 kV/cm. Depolarization fields generated by the redistribution of space charge, defects and dipole charges could be the mechanisms for the polarization decay after writing. For the infant period (within 10 s), depolarization fields could be the main contribution to the polarization loss. The depolarization field increases with increasing the retained polarization and it is time dependent. The long-time retention loss is attributed to the effects of redistribution of defect charges. This effect leads to a small decrease in the polarization by compensating the polarization charges when the redistribution of defect charges is driven by polarization. Due to the dielectric relaxation, the retained charge is generally less than the switched charge measured from the *P-E* hysteresis loop and the difference between them should be as small as possible to keep enough margin between the digits "1" and "0". Retention, like fatigue, is also dependent on the thickness of the film, nature of the electrodes, microstructure of the film, temperature, and the details of the test conditions. The understanding and improvement of the degradation behaviour of ferroelectric thin films will have an essential impact on the future success of these films for device applications. Detailed fatigue and retention measurements in close correlation with process conditions are being done to evaluate the merits of calcium bismuth ferrite thin films for memory applications.

IV. Conclusions

Highly (200)-oriented Ca-doped $BiFeO_3$ films having low leakage current were coherently grown at 500 °C on $LaNiO_3$ (LNO) buffer layer. All films have single phase perovskite-derivative structure (as detected by XRD) and show excellent ferroelectric properties. On the other hand, structural defects such as high porosity are responsible for the high leakage of the BFOCa30 on Pt. Among the studied films, the BFOCa030-LNO film exhibited a better microstructure with low leakage due to the local distortion and strain caused by the co-existing phases which is reflected in physical properties of the system. Leakage current data reveal that the electrical conduction in these samples occurs via oxygen vacancy hopping. Retention loss in ferroelectric capacitors is generally attributed to the presence of the internal electric field such as oxygen vacancy and anti-site defects. Due to its large spontaneous polarization, good fatigue and satisfying retention characteristics, the Ca-doped BFO films could be a suitable material for integrated device applications in ferroelectric random access memories.

Acknowledgments: The financial support of this re-

search project by the Brazilian research funding agencies CNPq 573636/2008-7, INCTMN 2008/57872-1 and FAPESP 2013/07296-2.

References

1. W.L. Li, T.D. Zhang, D. Xu, Y.F. Hou, W.P. Cao, W.D. Fei, "$LaNiO_3$ seed layer induced enhancement of piezoelectric properties in (100)-oriented (1-x)BZT-xBCT thin films", *J. Eur. Ceram. Soc.*, **35** (2015) 2041–2049.
2. A.Z. Simões, E.C. Aguiar, C.S. Riccardi, E. Longo, J.A. Varela, "Fatigue and retention properties of $Bi_{3.25}La_{0.75}Ti_3O_{12}$ films using $LaNiO_3$ bottom electrodes", *Mater. Character.*, **60** (2009) 353–356.
3. S.J. Chiu, Y.T. Liu, G.P. Yu, H.Y. Lee, J.H. Huang, "Enhancement of epitaxial $LaNiO_3$ electrode on the ferroelectric property of La-doped $BiFeO_3/SrTiO_3$ artificial superlattice structure by rf sputtering", *J. Crystal Growth*, **368** (2013) 1–5.
4. I. Shturman, G.E. Shter, A. Etin, G.S. Grader, "Effect of $LaNiO_3$ electrodes and lead oxide excess on chemical solution deposition derived $Pb(Zr_x,Ti_{1-x})O_3$ film", *Thin Solid Films*, **517** (2009) 2767–2774.
5. K.P. Rajeev, G.V. Shivashankar, A.K. Raychaudhuri, "Low-temperature electronic properties of a normal conducting perovkite oxide ($LaNiO_3$)", *Solid State Commun.*, **79** (1991) 591–595.
6. J.B. Goodenough, J.S. Zhou, "Orbital ordering in orthorhomibic perovskites", *J. Mater. Chem.*, **17** (2007) 2394–2405.
7. D.S.L. Pontes, A.J. Chiquito, F.M. Pontes, E. Longo, "Structural, dielectric, ferroelectric and optical properties of PBCT, PBST and PCST complex thin films on $LaNiO_3$ metallic conductive oxide layer coated Si substrates by the CSD technique", *J. Alloys Compd.*, **609** (2014) 33–39.
8. H. Naganuma, J. Miura, S. Okamura, "Ferroelectric, electrical and magnetic properties of Cr, Mn, Co, Ni, Cu added polycrystalline $BiFeO_3$ films", *Appl. Phys. Lett.*, **93** (2008) 052901.
9. P. Kharel, S. Talebi, B. Ramachandran, A. Dixit, V.M. Naik, M.B. Sahana, C. Sudakar, R. Naik, M.S.R. Rao, G. Lawes, "Structural, magnetic, and electrical studies on polycrystalline transition-metal-doped $BiFeO_3$ thin films", *J. Phys. C: Condens. Matter*, **21** (2009) 036001.
10. J. Liu, M.Y. Li, L. Pei, J. Wang, Z.X. Hu, X. Wang, X.Z. Zhao, "Effect of Ce and Zr codoping on the multiferroic properties of $BiFeO_3$ thin films", *Europhys. Lett.*, **89** (2010) 57004.
11. G.L. Yuan, S.W. Or, "Multiferroicity in polarized single-phase $Bi_{0.875}Sm_{0.125}FeO_3$ ceramics", *J. Appl. Phys.*, **100** (2006) 024109.
12. R. Ramesh, N.A. Spaldin, "Multiferroics: progress and prospects in thin films", *Nature Mater.*, **6** (2007) 21–29.
13. M. Fiebig, "Revival of the magnetoelectric effect", *J. Phys. D*, **38** (2005) R123.
14. L.F. Gonçalves, L.S.R. Rocha, E. Longo, A.Z. Simões, "Calcium doped $BiFeO_3$ films: Rietveld analysis and piezoelectric properties", *J. Mater. Sci.: Mater. Electron.*, **29** [1] (2018) 784–793.
15. B.G. Chae, S.J. Lee, S.H. Kim, Y.S. Yang, J.P. Kim, M.S. Jang. "Fatigue properties of $Pb(Zr_{0.52}Ti_{0.48})O_3$ thin films deposited on $LaNiO_3$ electrode", *J. Korean Phys. Soc.*, **32** (1998) 1438–1441.
16. B. Nagaraj, S. Aggarwal, R. Ramesh, "Influence of contact electrodes on leakage characteristics in ferroelectric thin films", *J. Appl. Phys.*, **90** (2001) 375–382.
17. C.C. Yang, M.S. Chen, T.J. Hong, C.M. Wu, J.M. Wu, T.B. Wu, "Preparation of (100)-oriented metallic $LaNiO_3$ thin films on Si substrates by radio frequency magnetron sputtering for the growth of textured $Pb(Zr_{0.53}Ti_{0.47})O_3$", *Appl. Phys. Lett.*, **66** (1995) 2643–2645.
18. M.S. Chen, T.B. Wu, J.M. Wu, "Effect of textured $LaNiO_3$ electrode on the fatigue improvement of $Pb(Zr_{0.53}Ti_{0.47})O_3$ thin films", *Appl. Phys. Lett.*, **68** (1996) 1430–1432.
19. Y.R. Luo, J.M. Wu, "$BaPbO_3$ perovskite electrode for lead zirconate titanate ferroelectric thin films", *Appl. Phys. Lett.*, **79** (2001) 3669–3671.
20. C.S. Liang, J.M. Wu, M.C. Chang, "Ferroelectric $BaPbO_3/Pb(Zr_{0.53}Ti_{0.47})/BaPbO_3$ heterostructures", *Appl. Phys. Lett.*, **81** (2002) 3624–3626.
21. Y. Hou, W. Li, T. Zhang, W.P. Cao, Y. Yu, T. Bai, W. Fei, "Large piezoelectric response induced by the coexistence of low-symmetry and self-polarization in Li^+-Nb^{5+}-doped $BiFeO_3$ polycrystalline films", *J. Phys. Chem. C*, **120** [11] (2016) 6246–6251.
22. W.L. Li, T.D. Zhang, Y.F. Hou, Y. Zhao, D. Xu, W.P. Cao, W.D. Fei, "Giant piezoelectric properties of BZT-0.5BCT thin films induced by nanodomain structure", *RSC Adv.*, **4** (2014) 56933–56937.
23. L.V. Costa, R.C. Deus, M.A. Zaghete, A. Ries, F. Moura, J.A. Varela, "Experimental evidence of enhanced ferroelectricity in Ca doped $BiFeO_3$", *Mater. Chem. Phys.*, **144** (2014) 476–483.
24. D.M. Rietveld, "A profile refinement method for nuclear and magnetic structures", *J. Appl. Cryst.*, **2** (1969) 65–71.
25. J.K. Kim, S.S. Kim, W.J. Kim, "Phase developments, microstructures, and ferroelectric properties of $BiFeO_3$ thin films prepared by a solution", *Integr. Ferroelect.*, **76** (2005) 103–109.
26. Y. Huang, K. Zhao, H.B. Lu, K.J. Jin, M. He, Z.H. Chen, Y.L. Zhou, G.Z. Yang, "Multifunctional characteristics of $BaNb_{0.3}Ti_{0.7}O_3/SiBaNb_{0.3}Ti_{0.7}O_3$/Si p-n junctions", *Appl. Phys. Lett.*, **88** (2006) 061919.
27. C. Quan, Y. Han, N. Gao, W. Mao, J. Zhang, J. Yang, X. Li, W. Huang, "Comparative studies of pure, Ca-doped, Co-doped and co-doped $BiFeO_3$ nanoparticles", *Ceram. Int.*, **42** (2015) 537–544.
28. L. Yao, X. Wu, S. Yang, Y. Zhang, "Structural and optical properties of Ca doped $BiFeO_3$ thin films prepared by a sol-gel method", *Ceram. Int.*, **43** (2017) S470–S473.
29. G. Albino, O. Perales-Pérez, B. Renteria-Beleño, Y. Cedeño-Mattei, "Effect of Ca and Ag doping on the functional properties of $BiFeO_3$ nanocrystalline powders and films", *MRS Proceedings*, **1675** (2014) 105–111.
30. P. Kumar, M. Kar, "Effect of structural transition on magnetic and dielectric properties of La and Mn co-substituted $BiFeO_3$ ceramics", *Mater. Chem. Phys.*, **148** (2014) 968–977.
31. Y. Zhang, W. Li, W. Cao, Y. Feng, Y. Qiao, T. Zhang, W. Fei, "Mn doping to enhance energy storage performance of lead-free 0.7NBT-0.3ST thin films with weak oxygen vacancies", *Appl. Phys. Lett.*, **110** (2017) 243901.
32. Y. Wang, C.W. Nan, "Enhanced ferroelectricity in Ti-doped multiferroic $BiFeO_3$ thin films", *Appl. Phys. Lett.*, **89** (2006) 052903.
33. T. Li, Y. Zhu, S.B. Desu, C.H. Peng, M. Nagata,

"Metalorganic chemical vapor deposition of ferroelectric $SrBi_2Ta_2O_9$ thin films", *Appl. Phys. Lett.*, **68** [5] (1996) 616–618.
34. A.L. Kholkin, V.V. Shvartsman, Y.A. Emelyanov, R. Poyato, M.L. Calzada, L. Pardo, "Stress-induced suppression of piezoelectric properties in $PbTiO_3$:La thin films via Scanning Force Microscopy", *Appl. Phys. Lett.*, **82** [13] (2003) 2127–2129.
35. M.M. Kumar, S. Srinath, G.S. Kumar, S.V. Suryanarayana, "Spontaneous magnetic moment in $BiFeO_3$ - $BaTiO_3$ solid solutions at low temperatures", *J. Magn. Magn. Mater.*, **188** [1-2] (1998) 203–212.
36. T.J. Park, G.C. Papaefthymiou, A.J. Viescas, A.R. Moodenbaugh, S.S. Wong, "Size-dependent magnetic properties of single-crystalline multiferroic $BiFeO_3$ nanoparticles", *Nano Lett.*, **7** [3] (2007) 766–772.
37. D. Lee, M.G. Kim, S. Ryu, H.M. Jang, S.G. Lee, "Epitaxially grown La-modified $BiFeO_3$ magnetoferroelectric thin films", *Appl.Phys. Lett.*, **86** [22] (2005) 222903–222905.
38. Y.H. Lee, J.M. Wu, C.H. Lai, "Influence of La doping in multiferroic properties of $BiFeO_3$ thin films", *Appl. Phys. Lett.*, **88** [1] (2006) 042903–042905.
39. C.J.M. Daumont, D. Mannix, S. Venkatesan, G. Catalan, D. Rubi, B.J. Kooi, J.T.M.D. Hosson, B. Noheda, "Epitaxial $TbMnO_3$ thin films on $SrTiO_3$ substrates: a structural study", *J. Phys.: Condens. Matter*, **21** [1] (2009) 182001–182005.
40. S.X. Dou, W.K. Yeoh, O. Shcherbakova, J. Horvat, J.H. Kim, A.V. Pan, D. Wexler, Y. Li, W.X. Li, Z.M. Ren, P. Munroe, J.Z. Cui, "Magnetic field processing to enhance critical current densities of MgB_2 superconductors", *Appl. Phys. Lett.*, **89** [20] (2006) 202504–202506.
41. X.B. Zhu, H.C. Lei, S.B. Zhang, X.D. Zhu, B.S. Wang, G. Li, X. Luo, W.H. Song, J.M. Dai, Y.P. Sun, D.Q. Shi, S.X. Dou, "Large magnetoresistance induced by surface ferromagnetism in A-type antiferromagnetic $La_{0.4}Sr_{0.6}MnO_3$ nanoparticles", *J. Magn. Magn. Mater.*, **321** [13] (2009) 2009–2014.
42. I. Sosnowska, T. Peterlin-Neumaier, E. Streichele, "Spiral magnetic ordering in bismuth ferrite", *J. Phys. C: Solid State Phys.*, **15** [23] (1982) 4835–4846.
43. F.Z. Huang, X.M. Lu, W.W. Lin, X.M. Wu, Y. Kan, J.S. Zhu, "Effect of Nd dopant on magnetic and electric properties of $BiFeO_3$ thin films prepared by metal organic deposition method", *Appl. Phys. Lett.*, **89** (2006) 242914.
44. J. Wang, A. Scholl, H. Zheng, S.B. Ogale, D. Viehland, D.G. Schlom, N.A. Spaldin, K.M. Rabe, M. Wuttig, L. Mohaddes, J. Neaton, U. Waghmare, T. Zhao, R. Ramesh, "Response to comment on "Epitaxial $BiFeO_3$ multiferroic thin film heterostructures"", *Science*, **307** (2005) 1203b.